Erratum 21 September 2017. See Erratum.

REVIEW

Quantum simulations with ultracold atoms in optical lattices

Christian Gross[1]* and Immanuel Bloch[1,2]*

Quantum simulation, a subdiscipline of quantum computation, can provide valuable insight into difficult quantum problems in physics or chemistry. Ultracold atoms in optical lattices represent an ideal platform for simulations of quantum many-body problems. Within this setting, quantum gas microscopes enable single atom observation and manipulation in large samples. Ultracold atom–based quantum simulators have already been used to probe quantum magnetism, to realize and detect topological quantum matter, and to study quantum systems with controlled long-range interactions. Experiments on many-body systems out of equilibrium have also provided results in regimes unavailable to the most advanced supercomputers. We review recent experimental progress in this field and comment on future directions.

Ultracold atoms offer remarkable opportunities for investigating quantum many-body problems that are relevant to fields as diverse as condensed matter physics, statistical physics, quantum chemistry, and high-energy physics (*1*). The high degree of controllability and new observation tools, which enable the detection of each individual atom, make ultracold atoms ideal as analog quantum simulators (*2*–*5*). The aim of such simulators is to solve difficult quantum many-body problems, especially those so complex that they cannot be solved even on today's most powerful classical supercomputers. One such problem is identifying ground states in the doped Fermi-Hubbard model, which is believed to play an important role in the explanation of high-temperature superconductivity (*6*–*8*). Others include out-of-equilibrium dynamics of quantum matter (*9*), where even the most advanced numerical methods cannot, for example, track the time dynamics of modestly sized two-dimensional strongly interacting systems.

Over the past 15 years, ultracold atoms have thus increasingly become a tool to investigate such complex strongly interacting quantum matter. Here, we discuss this progress, focusing on some of the latest experimental developments in the field. We concentrate on lattice-based quantum many-body systems, where the study of strongly correlated many-body physics started with the observation of the superfluid–Mott insulator transition for bosons (*10*). We note that a large amount of highly important work has also been carried out in the continuum, most notably the realization of the Bose-Einstein condensation–Bardeen-Cooper-Schrieffer crossover (*11*).

The optical lattices used in the experiments are typically formed by interfering several laser beams in order to realize a fully controllable periodic light structure meant to mimic the crystal lattice of a solid. Atoms can be trapped in such periodic light fields because of their polarizability, induced by the alternating electric field of the laser light (*12*). Such optical lattices offer a tremendous amount of versatility: Not only can the geometry, dimensionality, disorder, and depth of the lattice be controlled, lattices can also be engineered that carry effective magnetic fields (*13*) hundreds of times stronger than the strongest magnetic fields created in solid-state laboratories. This has enabled the investigation of topological quantum matter using the toolbox offered by ultracold atoms.

Fundamentally new observation tools based on quantum gas microscopes allow observation and control of quantum matter at the level of individual atoms. For example, being able to take single "snapshots" of a quantum many-body system provides access to intricate correlations between the constituent particles that are difficult to observe in other settings. Attributes such as magnetic correlation, hidden magnetism, and topological order can thus be probed in remarkably direct ways.

Finally, ultracold atoms can be highly isolated from the environment, allowing the exploration of fundamental phenomena in statistical physics. How does a closed, isolated quantum system establish a temperature and thermalize during its quantum evolution (*14*–*16*)? What type of closed quantum system fails to thermalize even after a long quantum evolution? Experiments with ultracold atoms and ions are central to exploring these fundamentally important research directions (*17*, *18*) that challenge the foundations of classical statistical physics and thermodynamics.

Quantum gas microscopes

The realization of quantum gas microscopes for bosonic rubidium atoms (*19*, *20*) was an important step forward for quantum simulations based on optical lattice systems. This technology enabled the single site–resolved detection of individual atoms, or more precisely of the local parity of the onsite atom number, in a two-dimensional optical lattice; thus, it realized the ideal tool for the precision readout of an ultracold atom–based quantum simulator (Fig. 1). The detection is based on in-trap laser cooling techniques pioneered earlier in large spacing optical lattices (*21*, *22*). Sufficiently many fluorescence photons scattered during the laser cooling are collected with a high-resolution imaging objective to allow the distinction of atoms on neighboring lattice sites. The laser cooling is crucial, as it prevents the atoms from hopping to nearby sites. With illumination times of a fraction of a second, the achievable signal-to-noise ratio is significantly higher than

High-resolution detection

Quantum gas microscopes enable the high-resolution fluorescence detection of atoms in single sites of a two-dimensional layer of optical lattices. The lattice spacing is small (typically 0.5 μm), such that the atoms can move through the lattice by tunneling with amplitude t. Additionally, they interact with each other with strength U when multiple atoms meet at the same lattice site. Quantum gas microscopy can provide access to single snapshots of the locally resolved atomic density in strongly correlated many-body systems.

A typical fluorescence image is shown at the lower left, where the fluorescence strength is encoded in the color scale from black over red to yellow. Thanks to the underlying lattice (white dots), the single site occupation can be faithfully reconstructed even in dense areas, whereas sparse individual atoms are directly visible.

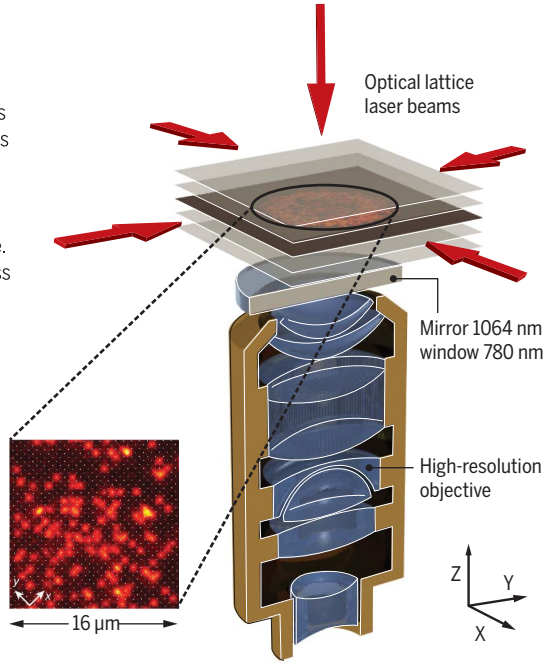

Fig. 1. Quantum gas microscopes. [Adapted from (*20*)]

GRAPHIC: ADAPTED BY V. ALTOUNIAN AND G. GRULLÓN/*SCIENCE*

[1]Max-Planck-Institut für Quantenoptik, 85748 Garching, Germany. [2]Germany Fakultät für Physik, Ludwig-Maximilians-Universität, 80799 Munich, Germany.
*Corresponding author. Email: christian.gross@mpq.mpg.de (C.G.); immanuel.bloch@mpq.mpg.de (I.B.)

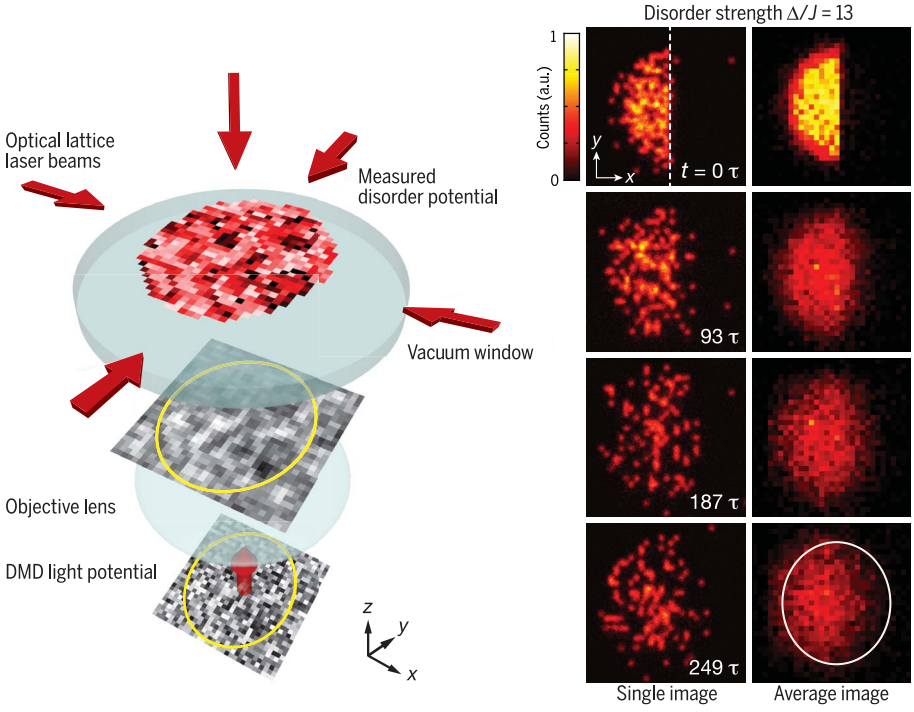

Fig. 2. Probing many-body localization in two dimensions. (**Left**) Almost arbitrary disorder potentials of light are projected onto an ultracold bosonic atom cloud. The quantum evolution of an initial nonequilibrium state can be tracked using a quantum gas microscope. (**Right**) The initial state is a domain wall of a bosonic Mott insulator ("half circle" in microscopy images). Even for long evolution times of ~250 tunneling times τ, the system fails to thermalize, indicated by the remnant domain wall still visible in the experiment. In contrast, a thermalized state would not carry any information about the initial state of the system (*68*).

with high-resolution absorptive imaging techniques (*23*). Electron beam microscopy offers even higher resolution but at lower detection efficiency (*24*). Soon after the single atom–resolved detection, precise manipulation techniques were added to the microscope toolbox, allowing for local control of individual atoms. Highly resolved intensity patterns were projected onto the atomic plane with the help of strongly focused beams or spatial light modulators (*25*–*27*). First experiments based on these techniques revealed the local entropy distribution of ultracold lattice bosons in the Mott-insulating phase and identified coherent particle-hole pairs as the remaining quantum fluctuations in the ground state close to the superfluid–Mott insulator transition (*20*, *28*, *29*).

Six years after the first demonstration of bosonic quantum gas microscopes, the technique was also successfully implemented for fermionic atoms (*30*–*34*). Owing to the electronic properties of the alkali atom fermions, more elaborate laser cooling methods, such as Raman-sideband cooling in three-dimensional optical lattices, needed to be developed to enable the site-resolved detection of individual fermions. Simultaneous detection of two hyperfine spin states has also been demonstrated (*35*, *36*), which provides unique access to correlations between the spin and charge (density) sectors (*37*).

Such single atom–resolved fluorescence imaging is not limited to alkali atoms. It has also been demonstrated for ytterbium, an atom with two valence electrons (*38*, *39*).

Strongly interacting bosons on a lattice

The Bose-Hubbard model, the first strongly correlated lattice model to have been realized with ultracold atoms (*10*), is still very prominent in experiments with ultracold atoms. It is realized when loading interacting bosonic atoms into optical lattices. Temperatures below the band gap are routinely obtained, such that its physics can be studied in the lowest band limit; extensions to higher bands are also possible (*40*). The simple but intriguing model contains three basic parameters: The nearest-neighbor tunneling strength t describes the motion of atoms in the lattice. The mutual interaction of atoms on the same lattice site is parametrized by U, and the (often harmonic) spatial confinement due to the laser beams results in a site i–dependent energy shift V_i. By reducing t/U, the ratio of the tunneling to the interactions, the system can be driven from the superfluid into the strongly correlated Mott insulating regime.

A prototypical example of a cold atom quantum simulation experiment is the observation of the Higgs amplitude mode in a two-dimensional Bose-Hubbard system (*41*–*44*). This excitation mode corresponds to the oscillations of the magnitude of the superfluid order parameter. It is predicted to exist in the vicinity of the superfluid–Mott insulator transition, where an emerging relativistic field theory describes the system. In traditional condensed matter systems, this mode had not been observed in two dimensions because a clean excitation method was missing. In a single-layer two-dimensional ultracold system, however, the modulation of the amplitude of the optical lattice potential naturally couples only to the magnitude of the superfluid order parameter, which made it possible to directly confirm the existence of the Higgs mode in two dimensions. Motivated by the cold atom experiments, recent work on low-dimensional materials has now also found evidence for the existence of the Higgs mode in these systems (*45*–*47*). The Higgs mode has also been observed in a quite different synthetic many-body system of a Bose-Einstein condensate loaded into two crossed optical cavities (*48*, *49*). This setting realizes a many-body system supporting a supersolid phase of matter, for which the effective field theory description also predicts an amplitude mode.

Magnetic phenomena are ubiquitous in solid-state physics and underlie many intriguing phenomena, some of which are still not fully understood theoretically. Frustrated magnets, where frustration leads to a large degeneracy of the system's ground state, are one example. Classical frustrated magnets can be realized in an ultracold atom system using shaken triangular lattices (*50*, *51*), where the local phase of the bosons represents a classical spin. The shaking parameters govern the phase winding, as they induce controlled complex tunneling elements between the different sites of a plaquette. Time-of-flight measurements provide access to the ensemble average of this classical spin, and thus the system state can be directly measured.

The simulation of quantum magnetism at first requires the identification of two local quantum states (the elementary magnets) representing the two spin states of the electrons, on which traditional magnetism is based. There are various possibilities to encode these two states in the ultracold lattice system, and different magnetic model Hamiltonians can thereby be realized. For example, the Ising model, where only one component of the spin vector interacts, has been realized in a tilted lattice by encoding the two spin states in the occupation difference between two neighboring sites (*52*). This method allowed for a single spin–resolved observation of the transition from a paramagnet, with all spins aligned in the direction of an external field, to the interaction-dominated Ising antiferromagnet with anti-aligned nearest neighbors. Nonequilibrium dynamics of such Ising chains have been studied by a controlled quench of the Hamiltonian parameters to the vicinity of this quantum phase transition (*53*); long-range tunneling resonances over several lattice sites have also been observed (*54*).

More complicated quantum spin models emerge when several directions of the spin vector contribute to the interaction between the elementary magnets. The special case of equal interactions in all directions is realized in the symmetric Heisenberg model. This model emerges for two-component

Erratum 21 September 2017. See Erratum.

bosons with equal interactions among all partners when the tunneling t in the lattice is suppressed in the Mott insulating phase. The two components can be defined by two Zeeman states in the hyperfine manifolds of the electronic ground state of the atoms. At unity filling in the lattice—that is, one atom per lattice site—the only remaining degree of freedom is the local orientation of this effective spin. The interactions between the spins turn out to be ferromagnetic and restricted to nearest neighbors only, resulting in the Heisenberg model $\hat{H} = -J\sum_i \hat{\mathbf{S}}_i \cdot \hat{\mathbf{S}}_{i+1}$. The interaction strength is given by the so-called superexchange coupling $J = 4t^2/U$ (*55*–*57*). Such a setting is realized with ^{87}Rb atoms in an optical lattice; the corresponding coherent spin dynamics were first observed locally (*58*, *59*) and later over several sites in one dimension (*26*).

Such two-component bosonic ^{87}Rb atoms in the lattice can be used to study spin transport microscopically. Quantum gas microscopes enable the direct tracking of the spin motion; a controlled initial state can be prepared, for example, by using local spin manipulation to reverse the direction of one (*60*) or two spins (*61*). The quantum motion of the spins through the chain results in entanglement generation between different sites, enabling direct detection of the propagation of the resulting entanglement wave (*60*). In the case of two initially flipped nearest-neighbor spins, bound magnon states are excited. These magnons consist of the flipped pair bound by the ferromagnetic Heisenberg interaction. They can regarded as the most elementary form of a magnetic soliton and were found to propagate as stable magnetic quasiparticles ballistically through the spin chain (*61*). At higher excitation energies, the quasiparticle picture is no longer useful and the exact theoretical solution is no longer easily accessible. Spin transport can, however, still be experimentally studied by starting from spin-spiral states, where the transverse magnetization vector linearly winds along the equator of the Bloch sphere as a function of position along the chain. Interferometric measurements of the transverse magnetization relaxation dynamics indicated diffusive spin transport at these high energies (*62*). Magnetization relaxation caused by superexchange and tunneling dynamics has also been studied in bosonic systems in two-dimensional lattices (*63*).

Magnetic many-body models still pose many open challenges that might be addressed by ultracold atom quantum simulators in the future. On the fundamental side, this includes models with frustrated ground states or topologically nontrivial models that emerge for elementary spins larger than ½. On the more technological side, the control of quantum spin arrays is a central resource in quantum computation.

Thermalization and many-body localization

The use of statistical physics and thermodynamics to describe classical and quantum many-body systems is ubiquitous. It is therefore of fundamental interest to understand why and when the principles of statistical physics hold, and whether there are genuine robust scenarios where this approach completely fails. For the first question, the notions of thermalization and ergodicity in quantum many-body systems are relevant. Thermalization occurs if local observables can be characterized by thermal expectation values after long time evolution. Thermalizing systems are sometimes also called ergodic, because during their evolution they explore all configurations in Hilbert space that are allowed by global conservation laws (*64*). To tackle the question of thermalization, the so-called eigenstate thermalization hypothesis has been proposed and tested both numerically and experimentally with increasing success (*14*–*16*, *65*). For most generic Hamiltonians, the hypothesis indicates that for an arbitrarily chosen high-energy many-body eigenstate of an isolated quantum system, any subsystem (after taking a trace over the rest of the system) will look thermal; that is, its density matrix will be given by a thermal density matrix. To some extent, this fact explains the tremendous success of quantum statistical physics and thermodynamics even for fully isolated quantum systems, whose initial state can be far away from any thermal equilibrium state but will eventually evolve into such a thermal state.

The second question, concerning when such scenarios fail, dates back to early work by Anderson (*66*). This question remained dormant and open for quite some time, but in 2006 a theoretical breakthrough was achieved that asserted that even for interacting quantum matter in disordered potentials, a new state of matter should exist (*67*) for which the conductivity strictly vanishes even at finite temperatures. This so-called many-body localized phase defies description by traditional statistical physics, as even for arbitrarily long evolution times, no thermal equilibrium state is reached. The associated phase transition from a thermalizing state to an insulating nonthermal state is a dynamical phase transition whose properties still remain in large part unclear (*17*, *18*).

Ultracold atoms (as well as ultracold ions) offer an ideal scenario to investigate these fundamental questions (*68*–*72*). Their minimal coupling to any thermal baths and the outside world makes them almost ideal isolated quantum systems, in contrast to normal low-temperature condensed matter experiments in dilution refrigerators, where the sample is a priori in thermal contact and in thermal equilibrium with the connected thermal reservoir.

Detection of spin correlations in Fermi-Hubbard systems

Spin-sensitive local detection of fermions

An optional spin-removal beam can be used to remove either of the two spin states encoded in two hyperfine states of the atoms before detection. In this way, either the spin or the density can be measured.

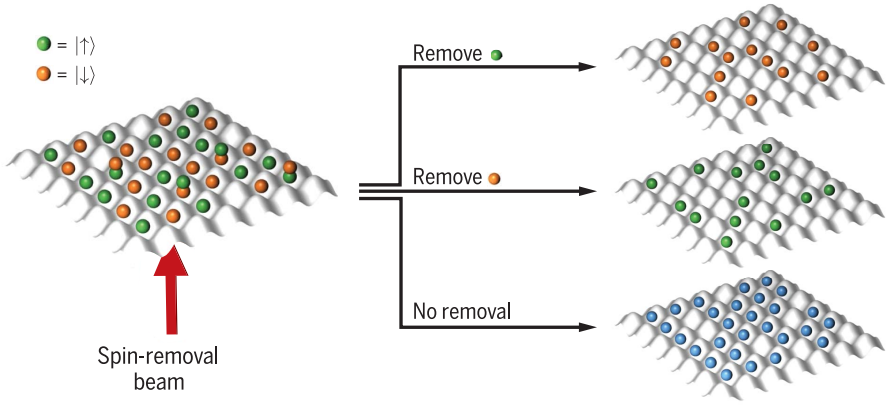

Detecting both spins: The image shows a fermionic Mott insulator characterized by a uniform central density.

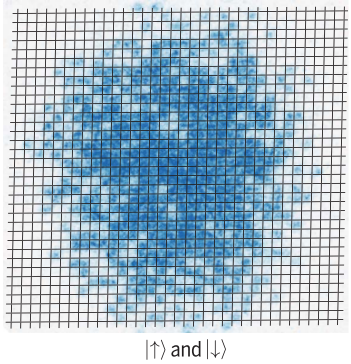

Detecting one spin: Spin correlations result in the apparent checkerboard pattern after removal of one spin component.

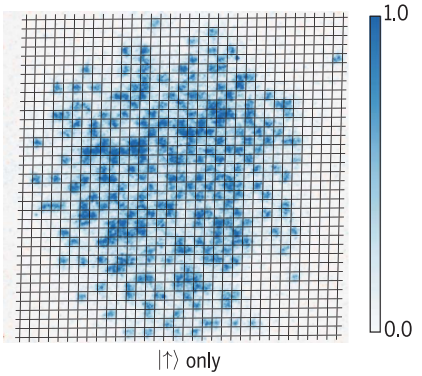

Fig. 3. Spin correlations in Fermi-Hubbard systems. [Bottom images adapted, with permission, from (*84*)]

Experiments probing such many-body localized phases of matter have so far typically proceeded by setting up a nonequilibrium initial state, such as an artificial charge density wave where only even lattice sites are occupied (*69*), a spatial domain wall boundary (*68*) (Fig. 2), or an atom cloud that received a momentum kick (*70*). The subsequent long-term evolution over as many as several hundred tunneling times showed that indeed no thermal steady state is reached and that the system retains a memory of the initial state even after a long-term quantum evolution (*68*, *69*). Experiments in one and two dimensions also suggest that the transition between the thermalizing and nonthermalizing phase takes place rather abruptly around a specific critical disorder strength. The experiments not only support the existence of such many-body localized phases in one and very likely also in two dimensions, but also indicated several other interesting effects. For example, domain wall experiments in two-dimensional systems found evidence for a diverging length scale around the transition and exhibited behavior strikingly different from that of an Anderson localized transition for noninteracting particles (*68*).

Many fundamental questions remain open: Quantum evolution to even longer times of thousands or tens of thousands of tunneling times would be quite useful in exploring the unique features of this novel phase transition and would help to distinguish the dynamics from those of classical glasses, which do thermalize, albeit on extremely long time scales. Complemented by theoretical research, there is much hope that this approach will unravel many of the secrets of the many-body localization transition, specifically to obtain a better understanding of the characteristics of this dynamical phase transition that defies classification by the usual schemes of statistical physics. In addition, the role of small thermalizing inclusions in a many-body localized system needs to be better understood, as these can crucially affect the stability of this intriguing phase in higher dimensions.

Fermions in optical lattices

One of the most active problems in optical lattice–based quantum simulation is the realization of the fermionic Hubbard model (*73*). This is motivated by the strong connection to high-temperature superconductors (*6*–*8*), where the Hubbard model is routinely used to model the effective electronic degrees of freedom. Binary spin mixtures of ultracold lattice fermions provide a defect-free and fully controlled implementation of the Hubbard model in which both the interactions and the doping can be continuously tuned. The former is controlled by the external magnetic field via Feshbach resonances (*74*), whereas the latter is determined by the atom number, setting the chemical potential in the trapped system. Ultracold atoms and quantum gas microscopes provide unique observation and manipulation opportunities, such as the characterization of the quantum state by local or nonlocal correlation functions that allow direct probes of hidden order parameters in a many-body setting (Fig. 3).

"It is...of fundamental interest to understand why and when the principles of statistical physics hold..."

As the interaction U/t is increased, finite-temperature, half-filled repulsively interacting Fermi-Hubbard systems undergo a crossover from the metallic to the Mott insulating state; in this context, half-filling means that the system is in the undoped regime of one-atom-per-site lattice filling and has equal numbers of both spin components. The Mott-insulating phase was observed in 2008 (*75*, *76*) using global observables such as the compressibility or the doublon fraction. With the use of high-resolution absorption imaging techniques, the equation of state in the density sector of the two-dimensional Hubbard model was measured (*77*) and extended density correlations were detected (*78*). The rich phase diagram of the Fermi-Hubbard model at low temperatures results from the interplay of the density (charge) and the magnetic degrees of freedom. Although the magnetic energy scale is given by the superexchange coupling J, even at higher temperatures $T > J$, magnetic short-range correlations—especially next-neighbor correlations—are present. Such nearest-neighbor correlations have been detected, first in lower dimensions (*79*, *80*) and later also in three-dimensional systems (*81*).

The realization of fermionic quantum gas microscopes was undoubtedly an important step forward toward the quantum simulation of the Fermi-Hubbard model in computationally inaccessible regimes. It resulted in the in situ observation of band and Mott-insulating states (*33*, *82*, *83*) and medium-range antiferromagnetic spin correlations (*36*, *84*–*87*), with the effective temperatures of the respective systems being at or only slightly below the superexchange energy scale. Very recent developments demonstrate the potential of these systems: In two dimensions, tailored optical traps have been used to realize entropy redistribution in the inhomogeneous system, as proposed in (*88*, *89*). Here, a large low-density region surrounding the higher-density core serves as an entropy reservoir. Because the systems can be manipulated while keeping the total entropy constant, the redistribution of entropy to the large reservoir leads to a decrease of the entropy in the

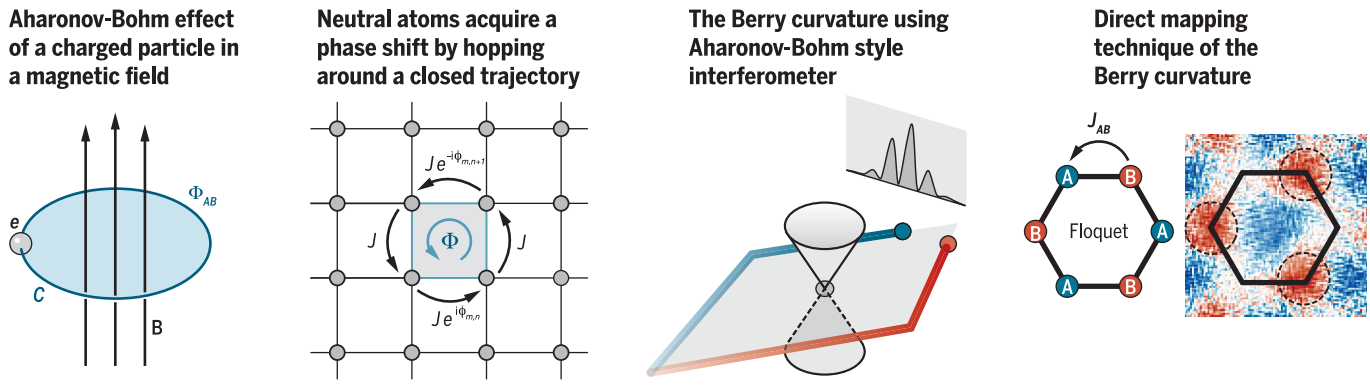

GRAPHIC: ADAPTED BY N. CARY AND A. KITTERMAN/*SCIENCE*

Fig. 4. Topological matter in cold atom systems. From left to right: Aharonov-Bohm effect of a charged particle in a magnetic field. When traveling around a closed loop enclosing magnetic flux Φ, the electron wave function acquires a phase shift proportional to Φ. Neutral atoms do not carry charge, but in engineered lattices with complex tunneling matrix elements between lattice sites, an atom hopping around a closed trajectory can also be made to pick up a phase shift, thereby emulating the effect of a magnetic field. [Adapted, with permission, from (*155*)] Berry curvature can be directly measured via an Aharonov-Bohm–style interferometer in momentum space. The wave packet of an atom is split and moved around a region including Berry curvature (e.g., Dirac cone with singular Berry flux located at the tip of the cone), such that the phase shift after interfering the wave packets will be proportional to the Berry flux enclosed in the interferometer. [Adapted from (*104*)] Alternatively, by rapidly switching the Hamiltonian between two band structures with coupled (weak lattice) and decoupled (strong lattice) sites enables direct mapping of the Berry curvature distribution in the Bloch bands via an alternative interferometric technique. [Adapted, with permission, from (*105*)]

Erratum 21 September 2017. See Erratum.

central part. This technique has been recently demonstrated, and effective core temperatures well below the superexchange scale have been realized. The resulting long-range correlations extended over the full extent of the low-entropy region (*90*). Simultaneously, progress on one-dimensional systems has also been made, and the direct detection of spin-charge multipoint correlations, which is important for the characterization of the Fermi-Hubbard system in the doped regime, has been reported (*37*). Measuring such multipoint correlators opens the path to the direct detection of many hidden and topological order parameters; in one-dimensional systems, these can be characterized by string correlation functions.

Artificial gauge fields and topology

The investigation and realization of novel topological phases of matter is of great current interest in condensed matter physics. Topological quantum phases of matter typically arise in a solid under the action of spin-orbit coupling or strong external magnetic fields (*91*–*93*). They defy the standard Landau classification of quantum phases in terms of a local order parameter; rather, they are typically characterized through a nonlocal topological invariant such as, for example, the Chern number. Realizing orbital magnetism that lies at the heart of many topological quantum phases with neutral cold atoms seems a priori impossible, as the atoms do not carry any charge. However, the effects of orbital magnetism can be mimicked by emulating the quantum mechanical effect of a charged particle in a magnetic field [i.e., the Aharonov-Bohm effect (*94*)] (see Fig. 4). A charged particle completing a closed-loop trajectory picks up a phase shift, which is proportional to the applied magnetic field strength. Optical lattice structures in which a neutral particle picks up a phase shift when traveling around a closed loop would emulate the effect of a charged particle in a magnetic field, and hence topological Bloch bands could arise (*95*, *96*).

Such phase shifts have been realized in two distinct ways, either by laser-induced tunneling or by lattice shaking. In the former case, tunneling between lattice sites is first suppressed by, for example, applying a strong potential gradient. The tunneling can then be restored by introducing a pair of laser beams, whose difference energy is tuned to bridge the energy difference between neighboring lattice sites induced by the strong potential gradient. However, the new tunneling matrix element can be complex-valued and may acquire a phase term, depending on the effective wave vector of the two laser beams. An atom completing a closed loop can therefore pick up a net phase shift, mimicking the Aharonov-Bohm phases picked up by electrons on closed trajectories in a magnetic field. Interestingly, and in contrast to condensed matter experiments, cold atom experiments thereby choose a certain gauge of the effective magnetic field. An alternative approach is based on lattice shaking, where the entire optical lattice is moved around in space on a circular trajectory, thereby realizing effective complex tunneling matrix elements in the resulting time-independent Floquet Hamiltonian (*50*, *97*, *98*). The former approach has been used to realize the Hofstadter model (*99*, *100*) for different flux values in optical lattices, whereas the latter was applied to realize staggered magnetic fluxes in triangular lattices (*50*) or the celebrated Haldane model (*101*) in a hexagonal lattice setup (*98*).

The geometry of the resulting topological Bloch bands is characterized by the so-called Berry curvature, defined over the magnetic Brillouin zone of the lattice $\Omega = i(\langle\partial_{q_x}u|\partial_{q_y}u\rangle - \langle\partial_{q_y}u|\partial_{q_x}u\rangle)$ (*102*, *103*), where $|u(q_x, q_y)\rangle$ denotes the Bloch wave functions in a single band of the lattice. This Berry curvature can be directly measured in a momentum-resolved way using an interferometric approach, similar to an Aharonov-Bohm interferometer, in which an atomic wave packet is split and coherently moved around a region in momentum space that has a finite Berry curvature distribution (*104*) (Fig. 4C). After recombining the two atomic wave packets, the wave function will have acquired a phase shift proportional to the enclosed Berry flux of the interferometer. Alternatively, bringing the atomic wave packet into a superposition of different energy bands has enabled direct mapping of the Berry curvature distribution in the Brillouin zone (*105*) (Fig. 4D).

The topological invariant—or Chern number—of the band is simply given by the integral of the Berry curvature over the entire Brillouin zone: $C = \frac{1}{2\pi}\int\Omega\, d^2q$. It can be accessed through the transverse bulk displacement of the atom cloud under the action of a force. Using semiclassical transport theory that includes the Berry curvature of the band (*103*), one finds that the transverse displacement of the cloud after one Bloch period $\tau_B = h/F_y a$ of the applied force F_y is given by $\Delta x = CA_{uc}/a$, where a denotes the lattice constant and A_{uc} is the area of the unit cell. In contrast to integer quantum Hall measurements in condensed matter, where the topological invariant can be determined through edge state transport and making use of the bulk-edge correspondence (*102*), here the Chern number can be measured directly through the bulk displacement of the atom cloud, yielding a value of $C = 0.99 \pm 0.05$ for the lowest energy band of the Hofstadter model (*106*).

A dynamical version of the integer quantum Hall effect, the Thouless charge pump (*107*), has also been realized in the context of ultracold atoms (*108*, *109*). Here, two lattices with different period are superimposed in one dimension with a phase ϕ characterizing the relative position of the two lattices. This phase, together with the momentum coordinate in one dimension, defines a two-dimensional parameter space, for which the quantum geometry of the system can again be defined using a generalized notion of the Berry curvature (*107*). Such Thouless pumps provide a robust pumping of charge, stable to imperfections, which is rooted in quantum mechanical tunneling motion of the particles and the topology of the band. Whenever the band is completely filled, one effectively integrates over the entire Berry curvature of the system, resulting in a quantized transport of charge (density) in the system. Such quantized transport was recently realized in (*108*, *109*), in addition to geometric pumping with no quantized charge (density) transport whenever the band is not entirely filled (*110*).

Ultracold atoms also offer possibilities for realizing synthetic dimensions (*111*), in addition to the physical dimensions present in the systems. Here, several internal states in an atom can be viewed as an extra dimension when coupled to each other, with the extension of the extra dimension determined by the number of substates available. In principle, the use of such synthetic dimensions allows exploration of topological quantum matter beyond three-dimensional settings. Synthetic dimensions have also been used to realize Hofstadter ribbons, in which the chiral edge states could be directly observed in the experiment (*112*, *113*).

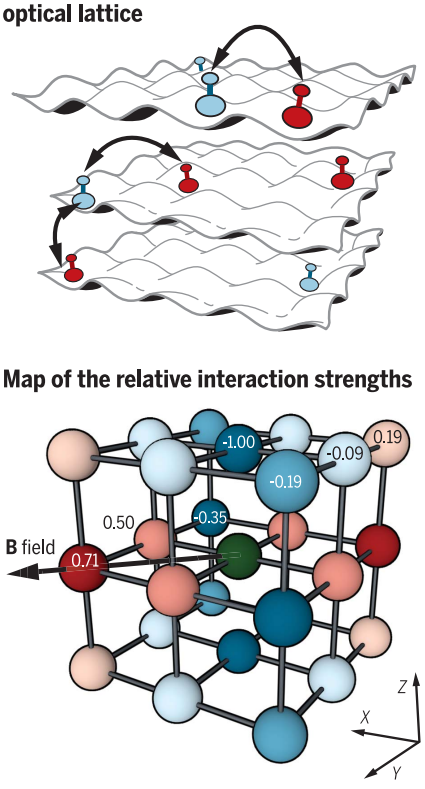

Fig. 5. Dipolar interactions. Top: Ultracold heteronuclear alkali molecules in their rotational and vibrational ground state can feature large electric dipole moments on the order of several debye. For a binary mixture of two different internal states of the molecules (red and blue), this can be used to realize sizable effective spin interactions over several lattice sites in optical lattices. With an externally set quantization axis (e.g., set by a magnetic **B** field), the dipolar interaction strength depends not only on the distance, but also on the direction of the vector connecting two molecules relative to the quantization axis. Bottom: Schematic indicating the relative interaction strength for nearby sites in a three-dimensional cubic optical lattice. [Adapted, with permission, from *Nature* (*129*), copyright 2013 Macmillan Publishers Ltd.]

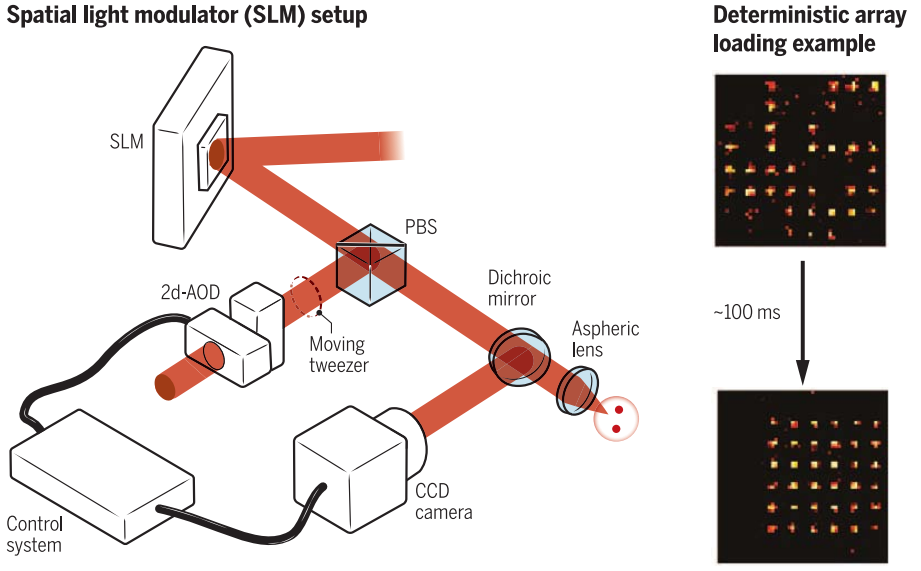

Fig. 6. Deterministic atom array preparation. Left: Schematic of the optical setup to generate arbitrary two-dimensional trap arrays via the spatial light modulator (SLM). The position of the moving tweezer, which sorts the initially randomly loaded atoms into the target array, is computer-controlled (control system) using an acousto-optical deflector (2d-AOD). The charge-coupled device (CCD) camera allows for nondestructive position monitoring of the atoms. Right: Example of one realization of deterministic array loading. The initially randomly loaded sample (top) is sorted in about 100 ms to a uniformly filled two-dimensional array (bottom). The detected atomic fluorescence is encoded from dark to light in the color scale; each spatially distinct area of high fluorescence signal corresponds to a single atom. [Adapted, with permission, from (*153*)]

Systems with dipolar interactions

In most cold atom experiments, atoms interact via short-range contact interactions. However, many-body systems with longer-range interactions are predicted to feature intriguing quantum phases and exhibit interesting dynamical behavior that can be very different from that of systems with contact interactions only (*114*–*116*). State-selective long-range interactions can be used to induce a direct spin-spin interaction (Fig. 5), which could also lead to exotic quantum magnetism featuring frustration or nontrivial topologies (*117*, *118*). Including the atomic motion as a relevant degree of freedom, extended Hubbard models (*119*) or spin-ice models described by dynamical gauge theories (*120*) might be realized.

Three approaches to inducing long-range interactions via ultracold atoms are under study. One is to use strongly magnetic atomic species such as chromium (*121*), dysprosium (*122*), or erbium (*123*), where the magnetic dipole-dipole interaction is sizable. In such a system, a shift of the superfluid–Mott insulator transition has been directly observed as a consequence of the dipolar interaction (*124*) and spin dynamics driven by the dipolar interactions have been studied (*125*). A second approach is based on ground-state polar molecules (*126*–*128*), for which the characteristic dipolar interaction has been observed in the dephasing dynamics of a collective spin ensemble of molecules (*129*). The third possibility is to make use of the extremely strong van der Waals interactions between Rydberg states (*130*). In laser-excited samples, this interaction exceeds all other energy scales on micrometer distances, leading to the Rydberg blockade effect (*131*, *132*), which results in the formation of spatially correlated structures during the excitation dynamics (*133*).

Crystalline low-energy states of the emerging spin model can be prepared using tailored optical excitation in combination with the spatial control over the shape of Mott insulators offered by quantum gas microscopes (*134*). This technique, however, is so far limited to rather small atomic samples of a few hundred atoms closely packed at a spacing of 0.5 μm in an atomic Mott insulator. Consequently, only a few many-body states actually participate in the excitation dynamics, whereas most configurations are far detuned owing to their high intrinsic interaction energy. This limitation can be avoided by using off-resonant Rydberg coupling. The ground state is only "dressed" by the Rydberg state, resulting in a tunable and much weaker dipolar interaction (*135*–*140*). The first attempts to observe effects attributable to these induced interactions failed in large three-dimensional samples because of interaction-induced resonance broadening (*141*–*143*). Nonetheless, coherent evolution of a Rydberg-dressed many-body system was recently demonstrated to be observable in small one- and two-dimensional systems; hence, this technique indeed allows for coherent interaction control (*144*, *145*) and is a promising basis for a future coherent quantum annealing platform (*146*).

For spin models coupled via state-selective long-range interactions, the motional degree of freedom of the atoms is frozen; that is, the atoms are pinned to their lattice sites. Hence, cooling to the ground state is not always required. Arrays of optical microtraps are an attractive alternative platform for such experiments because they require a less involved optical setup and feature much faster experimental cycle times than optical lattice–based experiments (*147*, *148*). Similar to quantum gas microscopes, these microtraps can be optically read out with single-atom precision. Furthermore, these setups allow for arbitrary geometrical arrangement of the microtraps in two dimensions—a great advantage when studying many-body models that, for example, are predicted to feature frustration (*117*). The realization of Rydberg spin models in such microtrap geometries has been demonstrated for the XY-model (*149*) as well as for the transverse Ising model (*150*). The loading of the microtrap arrays is a priori probabilistic, which hinders the deterministic production of larger atom arrays. This limitation has been overcome first for few-trap systems by laser-assisted blue shielding techniques (*151*, *152*) and recently in larger arrays by techniques that relocate the initially randomly placed atoms (*153*, *154*) into perfectly ordered and defect-free arrays (Fig. 6). These developments make the microtrap platform an ideal tool to study controlled spin systems interacting via Rydberg-induced interactions.

Outlook

Recent years have seen tremendous scientific progress in the field of quantum simulations with ultracold atoms. Quantum gas microscopes have revolutionized our way of controlling and probing many-body systems, atom-by-atom and with almost perfect control over the underlying potential. This has resulted in important advances in the realization of the low-temperature phases of the doped Fermi-Hubbard models; experiments now stand at a point where they are about to outperform even the most sophisticated quantum Monte Carlo algorithms on classical computers. Likewise, dynamical nonequilibrium simulations can be performed in regimes far beyond the reach of the most advanced supercomputers and are targeting fundamental questions in statistical physics and quantum information science. We believe that over the next years we will witness further improvements of cold atom–based quantum simulators; larger system sizes and longer coherent evolution times will enable even more complex quantum simulations. In addition, an enhanced local control over individual atoms and engineering of individual coupling strengths in a lattice will lead to highly versatile and programmable quantum simulators, allowing one to probe quantum matter in previously unexplored regimes with a unique degree of control. It will also establish cold atoms as a highly promising platform for coherent quantum annealing algorithms at the interface of quantum simulation and quantum computation with applications in the field of hard optimization problems. At the same time, the scientific reach of quantum simulations with cold atoms will very likely open up new paths in the field of dynamical quantum field theories relevant to quantum electrodynamics,

Erratum 21 September 2017. See Erratum.

quantum chromodynamics, and quantum chemistry; perhaps such simulations will even result in the discovery of new phases of matter.

REFERENCES AND NOTES

1. I. M. Georgescu, S. Ashhab, F. Nori, *Rev. Mod. Phys.* **86**, 153–185 (2014).
2. I. Bloch, J. Dalibard, W. Zwerger, *Rev. Mod. Phys.* **80**, 885–964 (2008).
3. M. Lewenstein *et al.*, *Adv. Phys.* **56**, 243–379 (2007).
4. D. Jaksch, P. Zoller, *Ann. Phys.* **315**, 52–79 (2005).
5. I. Bloch, J. Dalibard, S. Nascimbène, *Nat. Phys.* **8**, 267–276 (2012).
6. W. Hofstetter, J. I. Cirac, P. Zoller, E. Demler, M. D. Lukin, *Phys. Rev. Lett.* **89**, 220407 (2002).
7. P. A. Lee, N. Nagaosa, X.-G. Wen, *Rev. Mod. Phys.* **78**, 17–85 (2006).
8. K. Le Hur, T. M. Rice, *Ann. Phys.* **324**, 1452–1515 (2009).
9. A. Polkovnikov, K. Sengupta, A. Silva, M. Vengalattore, *Rev. Mod. Phys.* **83**, 863–883 (2011).
10. M. Greiner, O. Mandel, T. Esslinger, T. W. Hänsch, I. Bloch, *Nature* **415**, 39–44 (2002).
11. W. Zwerger, *The BCS-BEC Crossover and the Unitary Fermi Gas* (Springer, 2012).
12. R. Grimm, M. Weidemüller, Y. B. Ovchinnikov, *Adv. At. Mol. Opt. Phys.* **42**, 95–170 (2000).
13. N. Goldman, J. C. Budich, P. Zoller, *Nat. Phys.* **12**, 639–645 (2016).
14. T. Langen, R. Geiger, M. Kuhnert, B. Rauer, J. Schmiedmayer, *Nat. Phys.* **9**, 640–643 (2013).
15. T. Langen *et al.*, *Science* **348**, 207–211 (2015).
16. A. M. Kaufman *et al.*, *Science* **353**, 794–800 (2016).
17. R. Nandkishore, D. Huse, *Annu. Rev. Condens. Matter Phys.* **6**, 15–38 (2015).
18. E. Altman, R. Vosk, *Annu. Rev. Condens. Matter Phys.* **6**, 383–409 (2015).
19. W. S. Bakr, J. I. Gillen, A. Peng, S. Fölling, M. Greiner, *Nature* **462**, 74–77 (2009).
20. J. F. Sherson *et al.*, *Nature* **467**, 68–72 (2010).
21. K. D. Nelson, X. Li, D. S. Weiss, *Nat. Phys.* **3**, 556–560 (2007).
22. M. Karski *et al.*, *Phys. Rev. Lett.* **102**, 053001 (2009).
23. N. Gemelke, X. Zhang, C.-L. Hung, C. Chin, *Nature* **460**, 995–998 (2009).
24. T. Gericke, P. Würtz, D. Reitz, T. Langen, H. Ott, *Nat. Phys.* **4**, 949–953 (2008).
25. C. Weitenberg *et al.*, *Nature* **471**, 319–324 (2011).
26. T. Fukuhara *et al.*, *Nat. Phys.* **9**, 235–241 (2013).
27. P. Zupancic *et al.*, *Opt. Express* **24**, 13881–13893 (2016).
28. W. S. Bakr *et al.*, *Science* **329**, 547–550 (2010).
29. M. Endres *et al.*, *Science* **334**, 200–203 (2011).
30. L. W. Cheuk *et al.*, *Phys. Rev. Lett.* **114**, 193001 (2015).
31. E. Haller *et al.*, *Nat. Phys.* **11**, 738–742 (2015).
32. M. F. Parsons *et al.*, *Phys. Rev. Lett.* **114**, 213002 (2015).
33. A. Omran *et al.*, *Phys. Rev. Lett.* **115**, 263001 (2015).
34. G. J. A. Edge *et al.*, *Phys. Rev. A* **92**, 063406 (2015).
35. P. M. Preiss, R. Ma, M. E. Tai, J. Simon, M. Greiner, *Phys. Rev. A* **91**, 041602 (2015).
36. M. Boll *et al.*, *Science* **353**, 1257–1260 (2016).
37. T. A. Hilker *et al.*, *Science* **357**, 484–487 (2017).
38. M. Miranda, R. Inoue, Y. Okuyama, A. Nakamoto, M. Kozuma, *Phys. Rev. A* **91**, 063414 (2015).
39. R. Yamamoto, J. Kobayashi, T. Kuno, K. Kato, Y. Takahashi, *New J. Phys.* **18**, 023016 (2016).
40. G. Wirth, M. Ölschläger, A. Hemmerich, *Nat. Phys.* **7**, 147–153 (2010).
41. D. Podolsky, A. Auerbach, D. P. Arovas, *Phys. Rev. B* **84**, 174522 (2011).
42. L. Pollet, N. Prokof'ev, *Phys. Rev. Lett.* **109**, 010401 (2012).
43. D. Podolsky, S. Sachdev, *Phys. Rev. B* **86**, 054508 (2012).
44. M. Endres *et al.*, *Nature* **487**, 454–458 (2012).
45. D. Pekker, C. Varma, *Annu. Rev. Condens. Matter Phys.* **6**, 269–297 (2015).
46. D. Sherman *et al.*, *Nat. Phys.* **11**, 188–192 (2015).
47. A. Jain *et al.*, *Nat. Phys.* **13**, 633–637 (2017).
48. J. Léonard, A. Morales, P. Zupancic, T. Esslinger, T. Donner, *Nature* **543**, 87–90 (2017).
49. J. Léonard, A. Morales, P. Zupancic, T. Esslinger, T. Donner, Monitoring and manipulating Higgs and Goldstone modes in a supersolid quantum gas. arXiv:1704.05803 (2017).
50. J. Struck *et al.*, *Science* **333**, 996–999 (2011).
51. J. Struck *et al.*, *Nat. Phys.* **9**, 738–743 (2013).
52. J. Simon *et al.*, *Nature* **472**, 307–312 (2011).
53. F. Meinert *et al.*, *Phys. Rev. Lett.* **111**, 053003 (2013).
54. F. Meinert *et al.*, *Science* **344**, 1259–1262 (2014).
55. A. B. Kuklov, B. V. Svistunov, *Phys. Rev. Lett.* **90**, 100401 (2003).
56. L.-M. Duan, E. Demler, M. D. Lukin, *Phys. Rev. Lett.* **91**, 090402 (2003).
57. J. J. García-Ripoll, J. I. Cirac, *New J. Phys.* **5**, 76 (2003).
58. S. Trotzky *et al.*, *Science* **319**, 295–299 (2008).
59. S. Nascimbène *et al.*, *Phys. Rev. Lett.* **108**, 205301 (2012).
60. T. Fukuhara *et al.*, *Phys. Rev. Lett.* **115**, 035302 (2015).
61. T. Fukuhara *et al.*, *Nature* **502**, 76–79 (2013).
62. S. Hild *et al.*, *Phys. Rev. Lett.* **113**, 147205 (2014).
63. R. C. Brown *et al.*, *Science* **348**, 540–544 (2015).
64. D. A. Abanin, Z. Papić, *Ann. Phys.* **529**, 1700169 (2017).
65. L. D'Alessio, Y. Kafri, A. Polkovnikov, M. Rigol, *Adv. Phys.* **65**, 239–362 (2016).
66. P. W. Anderson, *Phys. Rev.* **109**, 1492–1505 (1958).
67. D. M. Basko, I. L. Aleiner, B. L. Altshuler, *Ann. Phys.* **321**, 1126–1205 (2006).
68. J. Y. Choi *et al.*, *Science* **352**, 1547–1552 (2016).
69. M. Schreiber *et al.*, *Science* **349**, 842–845 (2015).
70. S. S. Kondov, W. R. McGehee, W. Xu, B. DeMarco, *Phys. Rev. Lett.* **114**, 083002 (2015).
71. P. Bordia *et al.*, *Phys. Rev. Lett.* **116**, 140401 (2016).
72. J. Smith *et al.*, *Nat. Phys.* **12**, 907–911 (2016).
73. T. Esslinger, *Annu. Rev. Condens. Matter Phys.* **1**, 129–152 (2010).
74. C. Chin, R. Grimm, P. Julienne, E. Tiesinga, *Rev. Mod. Phys.* **82**, 1225–1286 (2010).
75. R. Jördens, N. Strohmaier, K. Günter, H. Moritz, T. Esslinger, *Nature* **455**, 204–207 (2008).
76. U. Schneider *et al.*, *Science* **322**, 1520–1525 (2008).
77. E. Cocchi *et al.*, *Phys. Rev. Lett.* **116**, 175301 (2016).
78. J. H. Drewes *et al.*, *Phys. Rev. Lett.* **117**, 135301 (2016).
79. D. Greif, T. Uehlinger, G. Jotzu, L. Tarruell, T. Esslinger, *Science* **340**, 1307–1310 (2013).
80. D. Greif, G. Jotzu, M. Messer, R. Desbuquois, T. Esslinger, *Phys. Rev. Lett.* **115**, 260401 (2015).
81. R. A. Hart *et al.*, *Nature* **519**, 211–214 (2015).
82. L. W. Cheuk *et al.*, *Phys. Rev. Lett.* **116**, 235301 (2016).
83. D. Greif *et al.*, *Science* **351**, 953–957 (2016).
84. M. F. Parsons *et al.*, *Science* **353**, 1253–1256 (2016).
85. L. W. Cheuk *et al.*, *Science* **353**, 1260–1264 (2016).
86. J. H. Drewes *et al.*, *Phys. Rev. Lett.* **118**, 170401 (2017).
87. P. T. Brown *et al.*, Observation of canted antiferromagnetism with ultracold fermions in an optical lattice. arXiv:1612.07746 (2016).
88. T.-L. Ho, Q. Zhou, *Proc. Natl. Acad. Sci. U.S.A.* **106**, 6916–6920 (2009).
89. J.-S. Bernier *et al.*, *Phys. Rev. A* **79**, 061601 (2009).
90. A. Mazurenko *et al.*, *Nature* **545**, 462–466 (2017).
91. S. M. Girvin, *The Quantum Hall Effect: Novel Excitations and Broken Symmetries* (Springer, 1999).
92. M. Hasan, C. Kane, *Rev. Mod. Phys.* **82**, 3045–3067 (2010).
93. X.-L. Qi, S.-C. Zhang, *Rev. Mod. Phys.* **83**, 1057–1110 (2011).
94. Y. Aharonov, D. Bohm, *Phys. Rev.* **115**, 485–491 (1959).
95. D. Jaksch, P. Zoller, *New J. Phys.* **5**, 56 (2003).
96. F. Gerbier, J. Dalibard, *New J. Phys.* **12**, 033007 (2010).
97. T. Oka, H. Aoki, *Phys. Rev. B* **79**, 081406 (2009).
98. G. Jotzu *et al.*, *Nature* **515**, 237–240 (2014).
99. M. Aidelsburger *et al.*, *Phys. Rev. Lett.* **111**, 185301 (2013).
100. H. Miyake, G. A. Siviloglou, C. J. Kennedy, W. C. Burton, W. Ketterle, *Phys. Rev. Lett.* **111**, 185302 (2013).
101. F. Haldane, *Phys. Lett. A* **93**, 464–468 (1983).
102. D. Thouless, M. Kohmoto, M. Nightingale, M. Den Nijs, *Phys. Rev. Lett.* **49**, 405–408 (1982).
103. D. Xiao, M.-C. Chang, Q. Niu, *Rev. Mod. Phys.* **82**, 1959–2007 (2010).
104. L. Duca *et al.*, *Science* **347**, 288–292 (2015).
105. N. Fläschner *et al.*, *Science* **352**, 1091–1094 (2016).
106. M. Aidelsburger *et al.*, *Nat. Phys.* **11**, 162–166 (2015).
107. D. Thouless, *Phys. Rev. B* **27**, 6083–6087 (1983).
108. M. Lohse, C. Schweizer, O. Zilberberg, M. Aidelsburger, I. Bloch, *Nat. Phys.* **12**, 350–354 (2016).
109. S. Nakajima *et al.*, *Nat. Phys.* **12**, 296–300 (2016).
110. H. I. Lu *et al.*, *Phys. Rev. Lett.* **116**, 200402 (2016).
111. A. Celi *et al.*, *Phys. Rev. Lett.* **112**, 043001 (2014).
112. M. Mancini *et al.*, *Science* **349**, 1510–1513 (2015).
113. B. K. Stuhl, H.-I. Lu, L. M. Aycock, D. Genkina, I. B. Spielman, *Science* **349**, 1514–1518 (2015).
114. T. Lahaye, C. Menotti, L. Santos, M. Lewenstein, T. Pfau, *Rep. Prog. Phys.* **72**, 126401 (2009).
115. M. A. Baranov, M. Dalmonte, G. Pupillo, P. Zoller, *Chem. Rev.* **112**, 5012–5061 (2012).
116. K. R. A. Hazzard *et al.*, *Phys. Rev. A* **90**, 063622 (2014).
117. A. W. Glaetzle *et al.*, *Phys. Rev. Lett.* **114**, 173002 (2015).
118. R. M. W. van Bijnen, T. Pohl, *Phys. Rev. Lett.* **114**, 243002 (2015).
119. E. G. Dalla Torre, E. Berg, E. Altman, *Phys. Rev. Lett.* **97**, 260401 (2006).
120. A. W. Glaetzle *et al.*, *Phys. Rev. X* **4**, 041037 (2014).
121. A. Griesmaier, J. Werner, S. Hensler, J. Stuhler, T. Pfau, *Phys. Rev. Lett.* **94**, 160401 (2005).
122. M. Lu, N. Q. Burdick, S. H. Youn, B. L. Lev, *Phys. Rev. Lett.* **107**, 190401 (2011).
123. K. Aikawa *et al.*, *Phys. Rev. Lett.* **108**, 210401 (2012).
124. S. Baier *et al.*, *Science* **352**, 201–205 (2016).
125. A. de Paz *et al.*, *Phys. Rev. Lett.* **111**, 185305 (2013).
126. K.-K. Ni *et al.*, *Science* **322**, 231–235 (2008).
127. J. G. Danzl *et al.*, *Science* **321**, 1062–1066 (2008).
128. J. Deiglmayr *et al.*, *Phys. Rev. Lett.* **101**, 133004 (2008).
129. B. Yan *et al.*, *Nature* **501**, 521–525 (2013).
130. M. Saffman, T. G. Walker, K. Mølmer, *Rev. Mod. Phys.* **82**, 2313–2363 (2010).
131. D. Jaksch *et al.*, *Phys. Rev. Lett.* **85**, 2208–2211 (2000).
132. M. D. Lukin *et al.*, *Phys. Rev. Lett.* **87**, 037901 (2001).
133. P. Schauß *et al.*, *Nature* **491**, 87–91 (2012).
134. P. Schauß *et al.*, *Science* **347**, 1455–1458 (2015).
135. L. Santos, G. V. Shlyapnikov, P. Zoller, M. Lewenstein, *Phys. Rev. Lett.* **85**, 1791–1794 (2000).
136. I. Bouchoule, K. Mølmer, *Phys. Rev. A* **65**, 041803 (2002).
137. G. Pupillo, A. Micheli, M. Boninsegni, I. Lesanovsky, P. Zoller, *Phys. Rev. Lett.* **104**, 223002 (2010).
138. N. Henkel, R. Nath, T. Pohl, *Phys. Rev. Lett.* **104**, 195302 (2010).
139. J. Honer, H. Weimer, T. Pfau, H. P. Büchler, *Phys. Rev. Lett.* **105**, 160404 (2010).
140. J. E. Johnson, S. L. Rolston, *Phys. Rev. A* **82**, 033412 (2010).
141. J. B. Balewski *et al.*, *New J. Phys.* **16**, 063012 (2014).
142. E. A. Goldschmidt *et al.*, *Phys. Rev. Lett.* **116**, 113001 (2016).
143. J. A. Aman *et al.*, *Phys. Rev. A* **93**, 043425 (2016).
144. J. Zeiher *et al.*, *Nat. Phys.* **12**, 1095–1099 (2016).
145. J. Zeiher *et al.*, Coherent many-body spin dynamics in a long-range interacting Ising chain. arXiv:1705.08372 (2017).
146. A. W. Glaetzle, R. M. W. van Bijnen, P. Zoller, W. Lechner, *Nat. Commun.* **8**, 15813 (2017).
147. M. Schlosser, S. Tichelmann, J. Kruse, G. Birkl, *Quantum Inform. Process.* **10**, 907–924 (2011).
148. F. Nogrette *et al.*, *Phys. Rev. X* **4**, 021034 (2014).
149. D. Barredo *et al.*, *Phys. Rev. Lett.* **114**, 113002 (2015).
150. H. Labuhn *et al.*, *Nature* **534**, 667–670 (2016).
151. T. Grünzweig, A. Hilliard, M. McGovern, M. F. Andersen, *Nat. Phys.* **6**, 951–954 (2010).
152. B. J. Lester, N. Luick, A. M. Kaufman, C. M. Reynolds, C. A. Regal, *Phys. Rev. Lett.* **115**, 073003 (2015).
153. D. Barredo, S. de Léséleuc, V. Lienhard, T. Lahaye, A. Browaeys, *Science* **354**, 1021–1023 (2016).
154. M. Endres *et al.*, *Science* **354**, 1024–1027 (2016).
155. M. Aidelsburger, thesis, Ludwig-Maximilians-Universität (2015).

10.1126/science.aal3837

Quantum simulations with ultracold atoms in optical lattices

Christian Gross and Immanuel Bloch

Science **357** (6355), 995-1001.
DOI: 10.1126/science.aal3837